

Transition-Metal-Centered Nine-Membered Boron Rings: $M\text{@}B_9$ and $M\text{@}B_9^-$ ($M = \text{Rh}, \text{Ir}$)

Wei-Li Li,[†] Constantin Romanescu,[†] Timur R. Galeev,[‡] Zachary A. Piazza,[†] Alexander I. Boldyrev,^{*,‡} and Lai-Sheng Wang^{*,†}

[†]Department of Chemistry, Brown University, Providence, Rhode Island 02912, United States

[‡]Department of Chemistry and Biochemistry, Utah State University, Logan, Utah 84322, United States

S Supporting Information

ABSTRACT: We report the observation of two transition-metal-centered nine-atom boron rings, $\text{Rh@}B_9^-$ and $\text{Ir@}B_9^-$. These two doped-boron clusters are produced in a laser-vaporization supersonic molecular beam and characterized by photoelectron spectroscopy and ab initio calculations. Large HOMO–LUMO gaps are observed in the anion photoelectron spectra, suggesting that neutral $\text{Rh@}B_9$ and $\text{Ir@}B_9$ are highly stable, closed shell species. Theoretical calculations show that $\text{Rh@}B_9$ and $\text{Ir@}B_9$ are of D_{9h} symmetry. Chemical bonding analyses reveal that these complexes are doubly aromatic, each with six completely delocalized π and σ electrons, which describe the bonding between the central metal atom and the boron ring. This work establishes firmly the metal-doped B rings as a new class of novel aromatic molecular wheels.

Photoelectron spectroscopy (PES) studies in conjunction with ab initio calculations have shown that small anionic boron clusters (B_n^-) are planar or quasi-planar for an extended size range at least up to $n = 20$.^{1–4} All planar boron clusters consist of a peripheral ring built from strong classical two-center-two-electron ($2c-2e$) σ -B–B bonds and one or more inner atoms, which are bound to the peripheral boron ring via delocalized in-plane σ - and out-of-plane π -bonds. The delocalized bonding renders multiple aromaticity and enhances the stability of the planar clusters. Two clusters, B_8^{2-} and B_9^- , stand out as perfectly symmetric D_{7h} - $B\text{@}B_7^{2-}$ and D_{8h} - $B\text{@}B_8^-$ molecular wheel-type clusters.^{5–7} In both systems, each peripheral boron atom contributes two valence electrons to the $2c-2e$ localized σ -bonds and one electron to participate in the delocalized σ - and π -bonding, while the central boron atom contributes all three valence electrons to delocalized bonding. In total, each cluster has six delocalized σ - and six delocalized π -electrons and therefore fulfills the Hückel rule ($4N+2$) for both σ - and π -aromaticity. A question arises: can we replace the central boron atom with a metal atom? If the metal atom can participate in the delocalized bonding, do these systems thereby form a new class of thermodynamically stable aromatic compounds?

In a recent study on isoelectronic substitution of a boron atom in B_8^- and B_9^- with aluminum we have shown that Al avoids the central position in AlB_7^- or AlB_8^- .⁸ Instead, both clusters have nonplanar umbrella-type structures, consisting of a positively charged Al ion bound to a B_7^{3-} or a B_8^{2-} counterion.

Transition metals with unfilled d-orbitals may be more favorable to bond with the peripheral atoms in a planar geometry if they have the right atomic size to fit inside an eight- or nine-membered boron ring. Indeed, a number of theoretical calculations have proposed substitution of the central B atoms in the B_8 and B_9 molecular wheels by a transition metal atom.^{9–13} In particular, the Fe-centered FeB_9^- cluster has been suggested to be doubly aromatic using both NICS and MO analyses.^{9,10} This conclusion is corroborated by chemical bonding analyses using the Adaptive Natural Density Partitioning (AdNDP) method.¹⁴

Recently, we proposed an electronic design principle that can predict stable transition-metal-centered planar boron clusters, $M\text{@}B_n^{k-}$.¹⁵ The design principle is based on the double aromaticity requirement and states that the total number of bonding electrons ($3n + x + k$) should be equal to the number of electrons in the peripheral bonds ($2n$) and the two sets of delocalized aromatic bonds ($6 + 6$) or $n + x + k = 12$, where x is the formal valence of the metal. Two metal-doped boron clusters have been observed recently, according to the design principle, D_{8h} - $\text{Co@}B_8^-$ and D_{9h} - $\text{Ru@}B_9^-$, in which the Co atom has a valence of 3 and the Ru atom has a valence of 2.¹⁵

In this communication, we report the investigation of two neutral transition-metal-centered nine-atom boron rings, $\text{Rh@}B_9$ and $\text{Ir@}B_9$ and their anions. Photoelectron spectra of $\text{Rh@}B_9^-$ and $\text{Ir@}B_9^-$ revealed a large energy gap for both species, suggesting that the neutral clusters are highly stable electronic systems. Ab initio calculations show that the anions are of C_{2v} symmetry due to the Jahn–Teller effect, whereas neutral $\text{Rh@}B_9$ and $\text{Ir@}B_9$ are closed-shell, doubly aromatic, and possess highly symmetric D_{9h} structures. The central metal atom in $M\text{@}B_9$, which has a valence of 3 and possesses six localized d electrons, is involved significantly in bonding with the B_9 ring.

The experiment was carried out using a magnetic-bottle PES apparatus equipped with a laser vaporization cluster source, details of which have been published elsewhere.¹⁶ In brief, the $M\text{@}B_9^-$ ($M = \text{Rh}, \text{Ir}$) clusters were generated by laser vaporization of a disk target containing isotopically enriched boron (96% ^{11}B , ~10% wt.) and transition metal (Rh or Ir, ~15% wt.), balanced by Bi, which acted as a binder and at the same time provided the Bi^- atomic anion as a convenient

Received: October 28, 2011

Published: December 13, 2011

calibrant for the PES apparatus. The clusters were entrained by a gas mixture containing 5% Ar in He supplied by two pulsed valves and underwent a supersonic expansion to form a collimated and vibrationally cold cluster beam.¹⁷ The anionic clusters were analyzed with a time-of-flight mass spectrometer. The clusters of interest were mass-selected and decelerated before being intercepted by the photodetachment laser beam operated at 193 nm (6.424 eV), 266 nm (4.661 eV), or 355 nm (3.496 eV). Photoelectrons were collected at nearly 100% efficiency by the magnetic bottle and analyzed in a 3.5 m long electron flight tube. The resolution of the apparatus $\Delta E/E$, was better than 2.5%, i.e. ~ 25 meV for 1 eV electrons.

The photoelectron spectra of RhB_9^- and IrB_9^- are found to be similar, as shown in Figure 1 at the three photodetachment

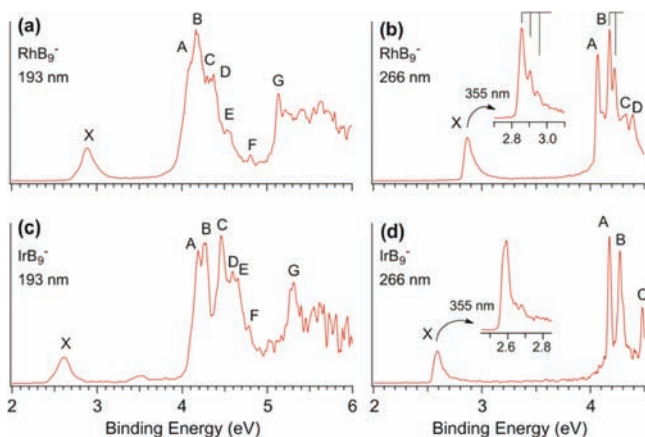


Figure 1. Photoelectron spectra of RhB_9^- and IrB_9^- at 355, 266, and 193 nm. The vertical lines in the 355 and 266 nm spectra of RhB_9^- indicate vibrational structures.

laser energies. Lower photon energies provide better spectral resolution while the high photon energy at 193 nm reveals more detachment transitions. The PES bands are labeled with letters (X, A, B, ...) and the vertical detachment energies (VDEs) are given in Table S1, Supporting Information (SI). In each spectrum, the X band represents the transition from the

anionic cluster ground state to the neutral ground state. The A, B, ... bands denote transitions to the excited states of the neutral.

The 355 nm spectrum (Figure 1b, inset) of RhB_9^- displays a nicely resolved short vibrational progression with an average spacing of $380 \pm 50 \text{ cm}^{-1}$. The 0–0 transition defines the adiabatic detachment energy (ADE) or the electron affinity of neutral RhB_9 at $2.86 \pm 0.03 \text{ eV}$. The short vibrational progression suggests that there is a very small geometry change between the anionic and neutral ground state. The 266 nm spectrum (Figure 1b) reveals four more features A, B, C, and D with VDEs of $4.07 \pm 0.03 \text{ eV}$, $4.18 \pm 0.03 \text{ eV}$, $4.33 \pm 0.04 \text{ eV}$, and $4.39 \pm 0.04 \text{ eV}$, respectively, following a large energy gap (1.21 eV) from band X. Both features A and B are very sharp, and feature B is vibrationally resolved with a spacing of $350 \pm 50 \text{ cm}^{-1}$. Two relatively weak features E (VDE: 4.54 eV) and F (VDE: 4.80 eV) are observed in the 193 nm spectrum (Figure 1a), followed by nearly continuous spectral features starting at band G at a VDE of $5.13 \pm 0.04 \text{ eV}$. No other definitive bands can be labeled in the high binding energy side due to the spectral congestion.

The 355 nm spectrum of IrB_9^- (Figure 1d, inset) exhibits a sharp peak with discernible vibrational structures. The 0–0 peak defines an ADE of $2.59 \pm 0.03 \text{ eV}$, which is also the electron affinity of the neutral IrB_9 cluster. Following a large energy gap (1.59 eV), a sharp and intense band A with a VDE of $4.18 \pm 0.03 \text{ eV}$ is observed in the 266 nm spectrum (Figure 1d). Two more sharp features, B and C, are also observed in the 266 nm spectrum with VDEs of $4.27 \pm 0.03 \text{ eV}$ and $4.48 \pm 0.03 \text{ eV}$, respectively. At 193 nm (Figure 1c), more transitions are observed. Features D and E are observed at $4.60 \pm 0.04 \text{ eV}$ and $4.65 \pm 0.04 \text{ eV}$, respectively. The weak feature F at 4.79 eV is similar to the corresponding feature in the 193 nm spectrum of RhB_9^- . Again, following an energy gap, a strong band G is observed at $5.31 \pm 0.04 \text{ eV}$, beyond which the signal-to-noise ratios are poor, but there appear to be continuous signals similar to the spectrum of RhB_9^- . There is a weak feature at 3.5 eV in the 193 nm spectrum of IrB_9^- in the band gap region. This feature is most likely due to autodetachment,^{18,19} because of its photon energy dependence.

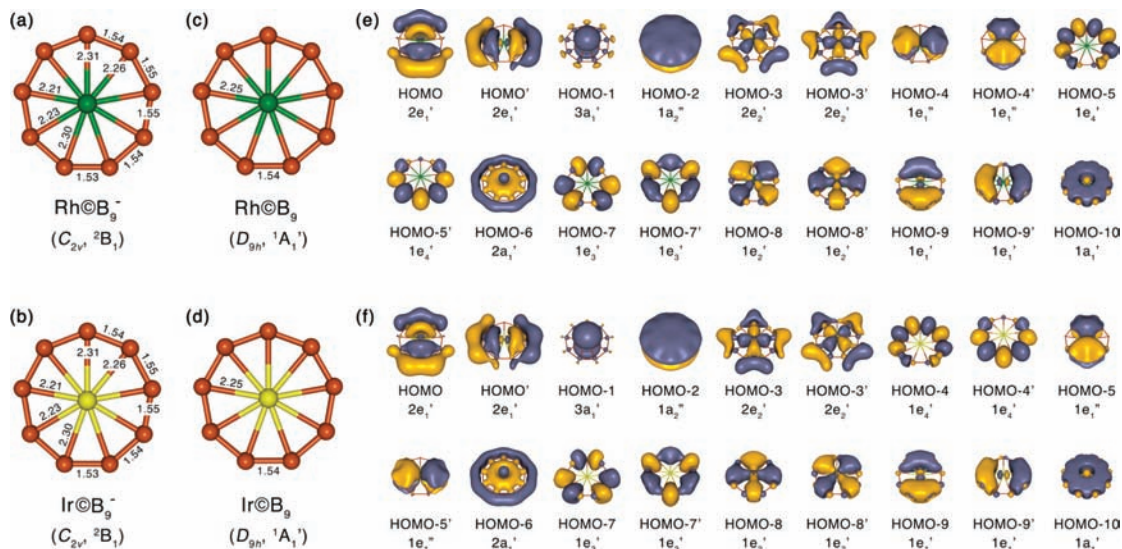


Figure 2. Optimized geometries of (a) Rh@B_9^- , (b) Ir@B_9^- , (c) Rh@B_9 , (d) Ir@B_9 and valence canonical molecular orbitals of (e) Rh@B_9 and (f) Ir@B_9 at PBE0/M/Stuttgart'97/B/aug-cc-pVTZ (M = Rh, Ir) level. Bond lengths are given in Å.

The large X–A gaps in the PES spectra of RhB_9^- and IrB_9^- suggest that their corresponding neutrals must be closed shell with large HOMO–LUMO gaps, and they should be electronically stable and chemically inert. The simplicity of the spectra and the sharpness of the various electronic bands indicate high-symmetry cluster species and minimum geometry changes during photodetachment transitions.

To aid the assignments of the PES spectra, we carried out ab initio calculations at different levels of theory. We first performed global minimum searches for the RhB_9^- and IrB_9^- clusters using the Coalescence Kick program³ at the PBE0/LanL2DZ level of theory. Low-lying isomers revealed by Coalescence Kick ($\Delta E < 40 \text{ kcal mol}^{-1}$ for RhB_9^- and $\Delta E < 55 \text{ kcal mol}^{-1}$ for IrB_9^-) were reoptimized using the PBE0/M/ Stuttgart'97/B/aug-cc-pVTZ ($M = \text{Rh or Ir}$) level of theory (Figures S1 and S2 in SI). To examine the possible multiconfigurational character of the global minimum C_{2v} species found by Coalescence Kick, we also optimized these geometries using the CASSCF method with the Ahlrichs pVDZ basis set for boron and the Stuttgart '97 basis set and ECP for Rh and Ir. Due to discrepancies in the order of ROHF molecular orbital symmetries of the two species, different active spaces were employed: CASSCF(7,8) for RhB_9^- and CASSCF-(9,9) for IrB_9^- . We found that for both species the Hartree–Fock configuration is dominant ($C_{\text{HF,RhB}_9^-} = 0.929$, $C_{\text{HF,IrB}_9^-} = 0.927$), and thus single determinant methods should provide a sufficient description of the ground-state wave functions.

Our geometry optimizations showed that the perfectly symmetric D_{9h} structures are minima on the potential energy surfaces of the neutral species, while the presence of an unpaired electron in the anion's doubly degenerate HOMO (the LUMO for neutral species) lowers the symmetry to C_{2v} due to the Jahn–Teller effect. The global minimum structures of the RhB_9^- and IrB_9^- clusters and the optimized perfectly symmetric Rh@B_9 and Ir@B_9 wheel-structures are shown in Figure 2a–d.

We then calculated the ab initio VDEs using four different methods to confirm that the C_{2v} structures are the global minima for RhB_9^- and IrB_9^- . PBE0/M/ Stuttgart'97/B/aug-cc-pVTZ and B3LYP/M/ Stuttgart'97/B/aug-cc-pVTZ ($M = \text{Rh, Ir}$) were used at their respective optimized geometries. VDEs were calculated also with the ROHF-UCCSD(T)^{20,21}/M/ Stuttgart'97/B/6-311+ G(2d) and EOM-CCSD(T)^{22–26}/M/ Stuttgart'97/B/6-311+G(2d)²⁷ methods at the PBE0/M/ Stuttgart'97/B/aug-cc-pVTZ optimized geometries. On the basis of the literature and our previous work with transition-metal-doped boron clusters,^{15,25} we believe that this basis set combination provides a reasonable balance between accuracy and computational efficiency for these approaches. EOM neutral excitation energies were used to offset the $\Delta\text{CCSD(T)}$ VDE for the lowest singlet state. The frozen core approximation was utilized in all CCSD(T) and EOM-CCSD(T) calculations. All DFT calculations were performed with the Gaussian 09 program.²⁸ CASSCF calculations were performed with the Gaussian 03 program.²⁹ All CCSD(T) calculations were performed with the tensor contraction engine module in NWChem version 6.0.³⁰

Because of the open-shell nature of the Rh@B_9^- and Ir@B_9^- anions, the detachment transitions are quite complicated, in qualitative agreement with the congested spectral features at the higher binding energy range. The computed VDEs are compared with the experimental data in Table S1, SI. For Rh@B_9^- , the first and second VDEs at CCSD(T) level are 2.87

and 4.22 eV, in good agreement with features X and A observed in the experimental spectra at 2.86 and 4.07 eV, respectively. The next two calculated VDEs correspond to the transition to the $^3\text{A}_2$ and $^3\text{B}_1$ final states with electrons detached from HOMO–2 ($6b_2$) and HOMO–3 ($8a_1$). We were not able to calculate these detachment channels at CCSD(T), but the VDEs calculated at the UPBE1PBE and UB3LYP are in good agreement with the experimental data (features B and C). The next three detachment channels correspond to singlet final states resultant of detachment from the fully occupied HOMO–1, HOMO–2, and HOMO–3 orbitals. These detachments correspond to the observed features D, E, and F. We were not able to calculate these values at UPBE1PBE and UB3LYP levels, but the VDEs calculated using EOM-CCSD(T), 4.40, 4.55, and 4.60 eV, are in reasonable agreement with the experimental data. The next major detachment channel is from HOMO–4 ($2b_1$), resulting in the $^3\text{A}_1$ final state. Electron detachment from HOMO–4 gives a VDE of 5.04 and 4.94 eV at UPBE1PBE and UB3LYP, respectively, compared to 5.13 eV in the experimental spectrum. As seen from Table S1, SI, the congested spectral features beyond the F band are consistent with the high density of detachment channels beyond HOMO–4. For Ir@B_9^- , the observed spectral features and assignments are very similar to those of Rh@B_9^- , as can be seen in Table S1, SI. In some cases, the spectra of Ir@B_9^- are better resolved, for example, the C band. Overall, for both species, the computational results are in excellent agreement with the experimental data, lending considerable credence to the molecular wheel structures for Rh@B_9^- and Ir@B_9^- .

The ground state of the two M@B_9^- anions is $^2\text{B}_1$ with C_{2v} symmetry due to the Jahn–Teller effect. The neutral ground state of M@B_9 is $^1\text{A}_1$ with perfect D_{9h} symmetry. The observed vibrational mode in the ground state transition should correspond to the distortion from the D_{9h} symmetry to the C_{2v} symmetry. The observed frequency of 380 cm^{-1} for Rh@B_9 is in excellent agreement with the calculated frequency for this mode, 386 cm^{-1} .

The neutral Rh@B_9 and Ir@B_9 clusters are valence isoelectronic to Ru@B_9^- , and they exhibit similar bonding patterns and strength.¹⁵ Valence canonical molecular orbitals of Rh@B_9 and Ir@B_9 are presented in e and f of Figure 2. Similar to Ru@B_9^- , we can understand the chemical bonding as follows. HOMO–2 ($1a_2''$) and HOMO–4 ($1e_1''$) of Rh@B_9 as HOMO–2 ($1a_2''$) and HOMO–5 ($1e_1''$) of Ir@B_9 are responsible for delocalized π -bonding (rendering π -aromaticity in the systems); HOMO ($2e_1'$) and HOMO–6 ($2a_1'$) of both clusters are responsible for delocalized σ -bonding (rendering their σ -aromaticity). HOMO–1 ($3a_1'$) and HOMO–3 ($2e_2'$) of both clusters are formed mainly by d electron lone-pairs of the central atoms and the remaining nine valence MOs are responsible for the B–B bonding in the circumference. Thus, both clusters are doubly aromatic, and the central metal has a formal valence of 3.

The current work has firmly established that transition-metal-centered monocyclic molecular wheels are a new class of highly stable and aromatic compounds. We have also confirmed our electronic design principle, which can be used to construct or screen other transition-metal–boron systems. With the availability of the transition-metal centers, which can accept ligands perpendicular to the molecular plane, this class of M@B_n complexes may be viable for chemical synthesis in the condensed phases.

■ ASSOCIATED CONTENT**■ Supporting Information**

Complete references 28 and 29, comparison of experimental VDEs with theoretical calculations at different levels of theory, optimized structures and relative energies (PBE0/M/Stuttgart'97/B/aug-cc-pVTZ, M = Rh or Ir) of the low-lying isomers of the RhB_9^- and IrB_9^- clusters. This material is available free of charge via the Internet at <http://pubs.acs.org>.

■ AUTHOR INFORMATION**Corresponding Author**

a.i.boldyrev@usu.edu; Lai-Sheng_Wang@brown.edu

■ ACKNOWLEDGMENTS

This work was supported by the National Science Foundation (DMR-0904034 to L.S.W., CHE-1057746 to A.I.B.). TeraGrid resources were provided by Pittsburgh Supercomputing Center. NWChem calculations were performed using the Chinook super computer at EMSL, a national scientific user facility sponsored by the DoE's Office of Biological and Environmental Research and located at Pacific Northwest National Laboratory. Computer time from the Center for High Performance Computing at Utah State University and an allocation of computer time from the Center for High Performance Computing at the University of Utah are gratefully acknowledged. T.R.G. thanks USU for the Vice President for Research Graduate Fellowship.

■ REFERENCES

- (1) Alexandrova, A. N.; Boldyrev, A. I.; Zhai, H. J.; Wang, L. S. *Coord. Chem. Rev.* **2006**, *250*, 2811.
- (2) Zhai, H. J.; Kiran, B.; Li, J.; Wang, L. S. *Nat. Mater.* **2003**, *2*, 827.
- (3) (a) Sergeeva, A. P.; Zubarev, D. Y.; Zhai, H. J.; Boldyrev, A. I.; Wang, L. S. *J. Am. Chem. Soc.* **2008**, *130*, 7244. (b) Sergeeva, A. P.; Averkiev, B. B.; Zhai, H. J.; Boldyrev, A. I.; Wang, L. S. *J. Chem. Phys.* **2011**, *134*, 224304.
- (4) (a) Huang, W.; Sergeeva, A. P.; Zhai, H. J.; Averkiev, B. B.; Wang, L. S.; Boldyrev, A. I. *Nature Chem.* **2010**, *2*, 202. (b) Kiran, B.; Bulusu, S.; Zhai, H. J.; Yoo, S.; Zeng, X. C.; Wang, L. S. *Proc. Natl. Acad. Sci. U.S.A.* **2005**, *102*, 961.
- (5) Zhai, H. J.; Alexandrova, A. N.; Birch, K. A.; Boldyrev, A. I.; Wang, L. S. *Angew. Chem., Int. Ed.* **2003**, *42*, 6004.
- (6) Alexandrova, A. N.; Zhai, H. J.; Wang, L. S.; Boldyrev, A. I. *Inorg. Chem.* **2004**, *43*, 3552.
- (7) Fowler, P. W.; Gray, B. R. *Inorg. Chem.* **2007**, *46*, 2892.
- (8) Galeev, T. R.; Romanescu, C.; Li, W. L.; Wang, L. S.; Boldyrev, A. I. *J. Chem. Phys.* **2011**, *135*, 104301.
- (9) Luo, Q. O. *Sci. China B* **2008**, *51*, 607.
- (10) Ito, K.; Pu, Z.; Li, Q. S.; Schleyer, P. v. R. *Inorg. Chem.* **2008**, *47*, 10906.
- (11) Li, S. D.; Miao, C. Q.; Guo, J. C. *Sci. China B* **2009**, *52*, 900.
- (12) Wu, Q. Y.; Tang, Y. P.; Zhang, X. H. *Sci. China B* **2009**, *52*, 288.
- (13) Pu, Z. F.; Ito, K.; Schleyer, P. V.; Li, Q. S. *Inorg. Chem.* **2009**, *48*, 10679.
- (14) Averkiev, B. B.; Wang, L. M.; Huang, W.; Wang, L. S.; Boldyrev, A. I. *Phys. Chem. Chem. Phys.* **2009**, *11*, 9840.
- (15) Romanescu, C.; Galeev, T. R.; Li, W. L.; Boldyrev, A. I.; Wang, L. S. *Angew. Chem., Int. Ed.* **2011**, *50*, 9334.
- (16) Wang, L. S.; Cheng, H. S.; Fan, J. W. *J. Chem. Phys.* **1995**, *102*, 9480.
- (17) Huang, W.; Wang, L. S. *Phys. Rev. Lett.* **2009**, *102*, 153401.
- (18) Wang, X. B.; Ding, C. F.; Wang, L. S. *J. Chem. Phys.* **1999**, *110*, 8217.
- (19) Li, J.; Li, X.; Zhai, H. J.; Wang, L. S. *Science* **2003**, *299*, 864.
- (20) Purvis, G. D.; Bartlett, R. J. *J. Chem. Phys.* **1982**, *76*, 1910.

- (21) Raghavachari, K.; Trucks, G. W.; Pople, J. A.; Head-Gordon, M. *Chem. Phys. Lett.* **1989**, *157*, 479.
- (22) Rowe, D. J. *Rev. Mod. Phys.* **1968**, *40*, 153.
- (23) Simons, J.; Smith, W. D. *J. Chem. Phys.* **1973**, *58*, 4899.
- (24) Sekino, H.; Bartlett, R. J. *Int. J. Quantum Chem.* **1984**, 255.
- (25) Stanton, J. F.; Bartlett, R. J. *J. Chem. Phys.* **1993**, *98*, 7029.
- (26) Levchenko, S. V.; Krylov, A. I. *J. Chem. Phys.* **2004**, *120*, 175.
- (27) Krishnan, R.; Binkley, J. S.; Seeger, R.; Pople, J. A. *J. Chem. Phys.* **1980**, *72*, 650.
- (28) Frisch, M. J. et al. *Gaussian 09*, Revision B.01; Gaussian, Inc.: Wallingford, CT, 2010. See the Supporting Information for the full citation.
- (29) Frisch, M. J. et al. *Gaussian 03*, Revision D.01; Gaussian, Inc.: Wallingford, CT, 2004. See the Supporting Information for the full citation.
- (30) Valiev, M.; Bylaska, E. J.; Govind, N.; Kowalski, K.; Straatsma, T. P.; Van Dam, H. J. J.; Wang, D.; Nieplocha, J.; Apra, E.; Windus, T. L.; de Jong, W. *Comput. Phys. Commun.* **2010**, *181*, 1477.